Broad ion beam cross-sectioning, microscopy, and image analysis of battery electrode morphology

Aamer Siddiqui

2022

LUTMDN / (TMMV-5342) / 1-48 / 2022

LUND UNIVERSITY

LTH

FACULTY OF ENGINEERING

MASTER THESIS

DIVISION OF PRODUCTION AND MATERIALS ENGINEERING

LUND UNIVERSITY

Academic Supervisor: Dmytro Orlov, Lund University
Industrial Supervisor: Tiva Sharifi and Matilda Klett, Scania CV AB
Examiner: Jan-Erik Ståhl, Lund University

Author: Aamer Mohammed Saleem Siddiqui
Lund, Sweden 2022

Avdelningen för Industriell Produktion
Lunds Tekniska Högskola
Lunds universitet
Box 118
221 00 Lund
Sverige

Division of Production and Materials Engineering
LTH, School of Engineering
Lund University
Box 118
SE-221 00 Lund
Sweden

Printed in Sweden
Media-Tryck
Lund University

Forward

I would like to thank my supervisors, Tiva Sharifi, Matilda Klett and Dmytro Orlov for their continuous support, direction and feedback during the entirety of the project. I am grateful that I was able to learn a lot and develop new skills. Apart from the technical knowledge, in particular I was able to learn a lot about project management skills from my supervisors, because of which we were mostly ahead of schedule. I am grateful for the conversations, discussions, career counselling, banter and a lot more than I can think of.

I am grateful to Scania and Lund University for providing me the tools and the necessary skills to work in a field of my interest. I also want to extend my gratitude to my colleagues at YTME at Scania and Dr.Dmytro's Research group for providing support for the thesis.

I want to thank my fellow Exjobbare, Felix, Christina, Mohammed, Sanna and Tobias for the frequent fika breaks, moral support, fun conversations and for making work much more enjoyable.

Finally, I want to thank my parents and my family for their continuous irreplaceable and unwavering support throughout the years.

Lund 2022-06-14

Aamer Siddiqui

Abstract

Lithium-ion batteries (LiB) are witnessing an increasing demand for electric vehicles. It provides a sustainable energy storage solution that is more efficient and ecofriendly than the fossil fuels. However, LiB are prone to ageing, which changes the dynamics of the electrochemical reactions over time and usage, and consequently affects its life and performance.. Ageing can manifest through multiple mechanisms that are also intertwined. Therefore, the understanding of these mechanisms is vital to designing more efficient and longer lasting batteries.

Physical characterization of the electrodes and other battery materials provides insights into the ageing mechanism, it helps visualize the effects or causes of the mechanism and can provide an aid to the electrochemical measurements. This project develops the technique of BIB-SEM and image analysis to study the electrode morphology and quantify the ageing mechanisms. Results from the method development show that there is an increase in the electrode dimensions with a ageing, there is also increase in particle cracking that is location based. The extent of particle cracking is higher, closer to the separator and gradually reduces closer to the current collector. This is also followed by an expected increase in porosity and reduction in tortuosity. The Li plating was also observed between the separator and graphite, the region consisted of filiform dendrites which extended into the separator. However, better imaging needs to be used to study the separator and the Li inclusions. The results also need to be compared against electrochemical measurements to correlate with the physical quantification.

Keywords: BIB, SEM, Li Plating, Particle cracking, Tortuosity, Image analysis

Table of Contents

Table of Figures

List of Tables

List of Abbreviations

LIB	**Lithium-ion battery**
EV	Electric Vehicle
EqD	Equivalent Diameter

SEM	Scanning Electron Microscopy
EDS	Energy Dispersive X-ray Spectroscopy
Acc.Voltage	Accelerating Voltage
LLI	Loss of Lithium Inventory
LAM	Loss of Active Material
CL	Conductivity Loss
SoC	State of Charge
SoH	State of Health
SEI	Solid Electrolyte Interphase
NMC	Nickle Manganese Cobalt Oxide
BSE	Backscatter Electron
SE	Secondary Electron

1. Introduction

In the recent times, the push towards sustainability and eco-friendliness has brought about an increase in demand for electric vehicles (EV). The main environmental challenges faced by the automotive industry is the carbon dioxide emissions, and therefore EV's have seemed to be the possible solution to mitigate this, in order to reduce the effect of climate change. Many solutions have been brought forward for electric vehicles, like metal hydride, Lithium ion, lead acid, however Li ion is currently being adopted at the fastest rate. Scania aims to electrify 50% of the total vehicle sales by 2030 [1]. This mass adoption implies that there needs to be considerable expertise and knowledge that is to be developed to implement this technology for mass production and to provide the customer with a reliable and efficient product. Therefore, the drive towards the Full electrification of the vehicle puts additional requirements on the battery. Vehicles are used in different conditions, ranging from temperature ranges, charging cycles, different power requirements, standstill conditions, driving habits and much more. All of these factors lead to the deterioration of the battery which undercuts its performance and shortens its life.

In EVs, Batteries are controlled and monitored by the battery management systems (BMS). This system provides feedback of the operational state of the battery, it optimizes performance and monitors and controls function from the cell, module, and the pack level. The BMS system works by using the inputs from the sensors on the current, voltage and temperature and other factors such as driving history to plan out the next step. This system is designed based on various models such as equivalent circuit model, thermal model, electrochemical models such as pseudo-two-dimensional and many more [2] .These models rely on parameters that help predict SoC (State of Charge) and SoH (State of Health) and other important metrics. However, with ageing these parameters tend to change and therefore would render the BMS system unreliable. Therefore, there is a need to understand the mechanism behind ageing and quantify the change in parameters that take place.

The understanding of batteries and their mechanisms are a imperative to providing a reliable commercial solution. It helps in designing better cells and provides insights for better modelling and prediction. Aging is quantified in electrodes by many mechanisms that are interrelated. The main effects of ageing seen from physical characterization are particle cracking, electrode volume expansion, Li plating, delamination, surface film formation, and

exfoliation. These factors can be quantified through observing cross-section of electrodes. This study aims to quantify these microstructural changes and features that are developed with aging.

1.1 Goal and Objective

The goal of the project is the following

1. To develop a methodology to use Broad Ion Beam-Scanning Electron Microscopy (BIB-SEM) for battery materials to analyze the cross section through Image analysis.
2. Develop a methodology to study Tortuosity in electrodes.
3. To observed and quantify Li plating

1.2 Scope

The primary focus of the thesis is limited to methodology development for BIB-SEM and Image analysis for quantifying aging mechanisms. The conditions of aging of cells and the electrochemical measurements are out of the scope of the thesis.

2. Theory

This section provides the theory and background on the working of the Lithium-ion battery, its material constituents, aging mechanism. It also discusses the tortuosity parameter and the theory behind the BIB.

2.1 LiB Principles

A cell is an electrochemical system that in principle converts chemical energy to electrical energy and vice versa. It consists of electrodes, separator, current collector, and electrolyte as the core components in Figure 1.

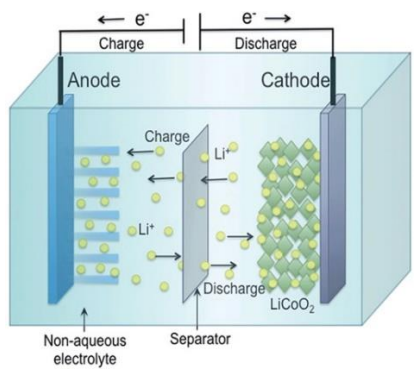

***Figure 1**. Li ion battery mechanism* [3]

The redox reaction drives the cell which is an electrochemical oxidation and reduction of the active material, where the electrons generated from this reaction is then collected by the current collector and the ions are transferred through the electrolyte. The Li ion are intercalated and extracted between the electrodes and the electrons are generated and consumed. The redox reaction is governed by a thermodynamic relationship and kinetics of the reaction. The reaction for Lithium Nickel Manganese Cobalt Oxide (NMC) electrode is shown in Table 1, where at the anode which has a electrode potential pf 200 mV vs Li/Li+ +, here the Li is oxidized to form Li ions which migrate to the cathode which has a nominal electrode potential of 3.8V through the electrolyte and are reduced at the cathode.

***Table 1**. Electrochemical reaction for NMC electrode based cell* [4]

Electrode	Electrochemical Reactions
Anode	$Li_nC_6 \rightleftharpoons Li_0C_6 + nLi^+ + ne^-$
Cathode	$Li_{m-n}(Ni_xMn_yCo_z)O_2 + nLi^+ + ne^- \rightleftharpoons Li_m(Ni_xMn_yCo_z)O_2$
Overall	$Li_nC_6 + Li_{m-n}(Ni_xMn_yCo_z)O_2 \rightleftharpoons Li_0C_6 + Li_m(Ni_xMn_yCo_z)O_2$

The cell is composed of active and non active material, where the active materials are directly involved in the redox reactions whereas the non active materials are passive. The active components are the electrodes whereas the non active are the separator, current collector, and the electrolyte. A brief description of each component is provided below.

- Electrode
    - Cathode

The electrodes are electrically and ionically conducting materials. NMC is currently widely used material for the cathode. It posses high capacity (~160–200 Ah/kg) , thermal stability and energy density [5]. The NMC can exist in various stoichiometric ratios leading to different properties for the electrodes. It is prone to structural degradation a chemical instability which decreases the cell performance [5].

    - Anode

Graphite has been a favorable material for the negative electrode for many applications. The reason for it is the low cost, abundance, good electrical conductivity, long life cycle and suitability of the material as host [6]. Graphite is composed of layers of graphene that are held together by Van der Waals forces. This enables the intercalation of Li ions across the prismatic surface. They also enable the formation of Li intercalation compounds of LiC_6 which provides theoretical specific and volumetric capacity of 372 mA h g^{-1} and 850 mA h cm^{-3}[7].

- Separator

The separator is an electrically resistive but ionically conductive porous membrane located between the two electrodes. It helps prevent contact between the two electrodes and consequently short circuiting. The separator is usually made of a polymeric compounds like polyolefin Polyethylene (PE), polypropylene [8] .

- Current Collectors

Current collectors facilitate the transfer of electrons into the external circuit. These are present as thin foils on the sides of both the negative and positive electrodes. These are usually aluminum for the positive and copper for the negative current collectors. They possess high electrical conductivity and stability in electrochemical reactions. Current collectors also enable heat transfer away from the electrode and provide mechanical strength to the electrodes.

2.2 Electrode Aging

Cell aging is the deterioration or gradual diminishing of the performance or health of a cell which is caused by irreversible physical and chemical changes that take place with time. There are various causes for ageing, such as temperature, mechanical stress, time, current loads, charging rates and many more. The understanding of cause and effect of these changes provides insights to design, manufacture and implement better batteries. Therefore, it is important to study the mechanisms and its effects behind ageing.

The major ageing modes can be divided into three broad categories as follows

1. Loss of Lithium inventory
   This is associated with the loss of cyclable Li ions, which are consumed by side reactions, Solid Electrolyte Interphase (SEI) formation, Li plating and others. This can lead to capacity, and power fade due to film formation [9].
2. Loss of active material
   The loss of active material is associated with the inability of both positive and negative to intercalate Li ions. It is cased by particle cracking, loss of contact, structural damage, and others. This can lead to capacity and power fade [9].
3. Conductivity Loss
   This mode is associated with the loss in the conductivity with delamination and degradation of current collector or binders [9].

   Mechanism

This section discusses the different ageing mechanisms for each material. The mechanisms affecting the battery aging are numerous and intertwined as shown in Figure 2. However, this study will focus on the major aging mechanisms and their effects that are possible to quantify through morphology changes.

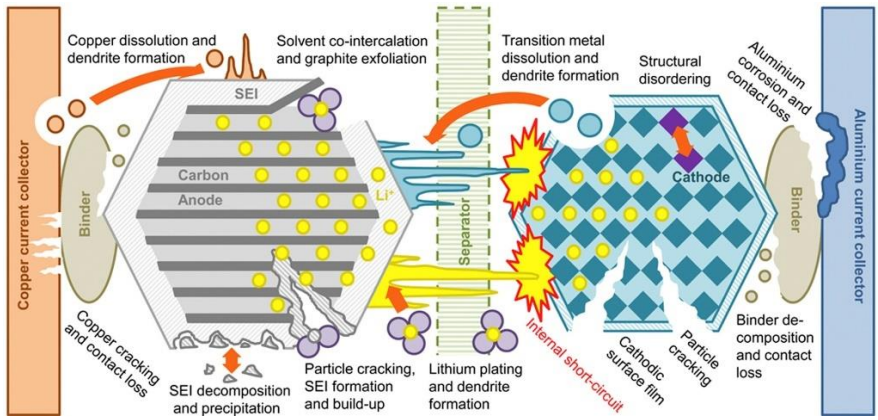

Figure 2. Ageing Mechanism in Li ion cells [9]

Cathode

Cathode experiences majority of the degradation mechanisms originating from the interaction of electrolyte and electrode. Some of the mechanisms are as follows

1. Structural Factors

Structural degradation is caused from phase transitions and structural disordering, resulting in capacity and voltage fade. The mechanism behind this degradation is the repeated intercalation and extraction of Li ions that lead to a volume expansion [10][11]. This in turn induces stresses and strains in the lattice, causing phase transitions and crystal distortion. Additionally, this causes particle cracking which again leads to further capacity fade due to loss of contact [12]. The particle cracking leads to increase in surface area with the electrolyte therefore increasing degradation reaction.

2. Surface effects/ reactions

Surface reactions arise from the interaction of the electrode and the electrolyte. This causes electrolyte decomposition and gas evolution which is observed at high temperatures and high voltage applications [13]. The film formation from the decomposition increases the impedance of the cell [14].

3. Active material dissolution

Dissolution of metallic oxides occurs into the electrolyte at high temperatures. The metal ions tend to travel towards the anode and are consumed in the SEI layer [12]. This accelerates the electrolyte decomposition and leads to anode self-discharge. In the case of NMC electrode, it is expected that this effect is minimal, although at high potential

all the constituent metals will dissolve. This means that it will lead to LLI through the deposition of the metal species in the SEI layer and Mn is the main contributor to this loss when deposited in the anode [15].

Anode

1. Structural factors
   Structural degradation, similar to the cathode is caused by the repeated insertion and extraction of the Li ions which causes volume expansion. This expansion leads to diffusion induced stresses and propagation of fractures in the cathode. High SoC and high C-rate cycling induces these strains on the graphite lattice [16]
2. Formation of Surface Layer
   Anode when operated outside of the electrochemical stability window of the electrolyte gives rise to reactions that consume Li ions, decomposes the electrolyte, and produces deposits. This causes the formation of the SEI layer which is a passivation layer that is located on the anode surface, where it is ionically conductive but electrically insulating and hence provides a protective cover [12]. However this layer also consumes cyclable lithium and the electrolyte and therefore leads to capacity loss [11]. The metal ions from the dissolution are also deposited in this region.
3. Li plating
   Li plating is the deposition of metallic Lithium on the surface of the electrode. This section will explain its formation, cause and detection techniques.
   I. Causes
      Li plating is a result of the limitation in the diffusive flux in the intercalating spaces of the anode. The diffusion of Li ions depends on concentration gradient and temperature. Li plating is caused by many factors such as low temperatures, high charging rates and high SoC. The potential for lithiated graphite is slightly above that of the Li formation. Therefore, to attain high lithiation rates, a large potential drop provides a thermodynamically favorable condition for plating to form. This is exacerbated by the concentration gradient of Li ions and the ohmic losses of the electrolyte at higher rates. [17][18].
   II. Risks
      Li plating in general is a reversable reaction, although when Li dendrites lose contact with the active material it forms irreversible Li dead regions, moreover these dendrites can grow into the separator and cause short circuiting. This Li

plating also reacts further with the electrolyte and leads to the growth of the SEI which further leads to capacity fade[18], [19].

2.3 Physical characterization of Ageing mechanism

This section will focus on surveying current findings and techniques to quantify, evaluate, and explain ageing mechanism in the scope of physical characterization.

A plethora of techniques have been used to study the electrode morphology ranging from micro level optical microscopy to high resolution Transmission electron microscopy (TEM) studies. Optical microscopy has been used widely to monitor and quantify Li dendrites with ageing, this technique is easily available and relatively practical for in-situ studies [20]–[22]. At a higher resolution, In situ and ex situ SEM studies are used to study Li plating, deposition, morphology, and processes. This is used in conjunction with cross sectioning techniques such as BIB or Focused ion beam (FIB), which is used to study particle cracking, phase transformations and crystal distortions. Chiara et al used Focused ion beam secondary ion mass spectrometry (FIB-SIMS) technique to study the distribution of Li in the constituents although the author acknowledged this only provides semi-quantitate results [23]. The structure of Li growth had been imaged with this technique by Uhlmann et al , it was also used to visualize the particulate structure of the Li deposit by Rauhala et al [24], [25].

TEM studies have been a strong tool to study electrode degradation, due its high resolution, sensitivity and versatile capability to study material composition, phases and structures [26]. It was used to measure the thickness of the SEI layer during lithium plating and stripping. It was also used to study formation of dead lithium by Zeng et al [27]. The other technique widely used is Nuclear Magnetic Resonance Spectroscopy (NMR), it provides the ability to extract structural information with high level of detail and accuracy. This has been used measure the Li plating at different SoC and temperatures, it has also been used in-situ to record the Li deposition rates at sub-zero temperatures[28], [29].

Synchrotron radiation has been used to study battery materials, due to its ability to provide high power and flux and the ability to perform in situ studies [30].It helps provide insight and answers to fundamental questions about the behavior and functioning and underlying mechanisms. Techniques such as X-ray powder diffraction (XRD) and X-Ray absorption spectroscopy (XAS) have been widely used on battery material. XAS is used since the energy shift of the spectra is used to provide insight into the

degradation mechanism of the NMC [31]. Synchrotron radiation X-ray tomographic microscopy (SRXTM) was also used to acquire 3D representation of the microstructure to perform diffusion simulations to calculate tortuosity [32]. This provides ultra-higher resolution tomography compared to the widely used X-ray computed tomography (XCT).

To summarize, most of the techniques used are either expensive to acquire or have limited access and are owned by research institutes and universities. Therefore, this thesis looks into employing the use of BIB-SEM technique that is already available at Scania AB to study battery materials and their aging.

2.4 Tortuosity

The understanding of battery morphology and microstructure is imperative to the designing better cells. One of the characteristic parameters of the microstructure is the Tortuosity. It is an essential factor in the mass transport of porous electrodes; therefore, it is a crucial parameter in cell modelling and design. Tortuosity is defined geometrically as the fraction of the shortest path over the distance between two points in the porous microstructure [33]. This definition is built on the bases that there can only be one shortest path in a porous microstructure, however this pathway is not preferential diffusion path of certain molecules of gases. The definition of tortuosity has been a widely discussed topic, however this study will focus on the geometrical tortuosity obtained from 3D reconstruction of the microstructure.

One of the fundamental methods to calculate tortuosity is through a porosity/tortuosity relationship where the knowledge of one factor such as the porosity can help calculate tortuosity. The most widespread method this relationship is the Bruggeman relationship which is expressed by the following equation

$$\tau_{\text{Bruggeman}}{}^{2} = \varepsilon^{1-\alpha} \qquad \textit{Equation 1.}$$

Here the τ is the tortuosity, ε is the porosity and the α is the Bruggeman coefficient. There have been many additions to this relationship since it does not confirm well with the experimental results, this is still an ongoing research area to validate the relationship. Tortuosity can be measured in multiple ways, one of which is 3D reconstruction of the microstructure through CT scan or synchrotron X-ray tomography which is discussed in the previous sections. The 3D reconstruction is then simulated for mass transfer and the Bruggeman exponent is calculated. There are multiple opensource solutions for this measurement, this study will employ the use of the TauFactor application for MATLAB [34].

2.5 Broad Ion Beam Milling Principles

Surface characterization relies on the quality of the surface, which can drastically affect the results from the characterization techniques. Broad Ion Beam is a tool used to cross section or polish surfaces of material for further analysis. It mitigates the drawbacks from mechanical polishing, which leaves the surface with crystal lattice damage, plastic deformation and contamination, it can also introduce heat to the sample and lead to oxidation of the surface [35]. BIB improves on this and also enables a wider variety of materials to be polished, it includes soft and hard materials from paper to metals and in addition it can polish a sandwich of different materials in the same specimen.

BIB milling works by producing accelerated Argon ions from an ion source which bombards the desired surface and ejects the material atomic layer by layer [35]. This ion source is a penning system which works by applying high voltage between the cathode and anode to produce the plasma, which then accelerates the ion in the in the plasms by applying a negative voltage between cathode A and B and the accelerating electrode.

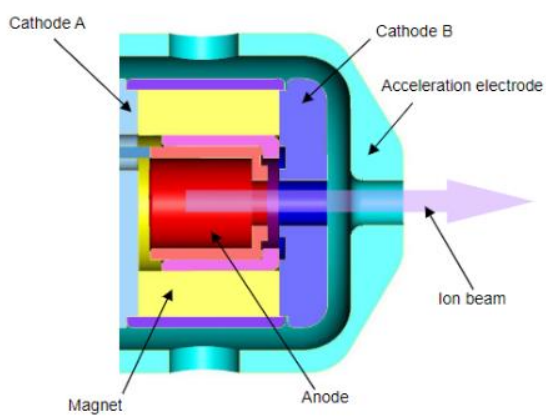

Figure 3. Ion source parts[36]

The continuous bombardment can cause the conversion of the kinetic energy of the ions into heat on the specimen. This heat needs to be removed if the specimen is sensitive. The BIB enables both crossection and flat milling. Where crossection milling involves only polishing or milling off the specimen crossection. This is carried out by using a mask that blocks off a apart of the beam from interacting with the surface and only allows the milling of the desired surface which is illustrated in Figure 4.

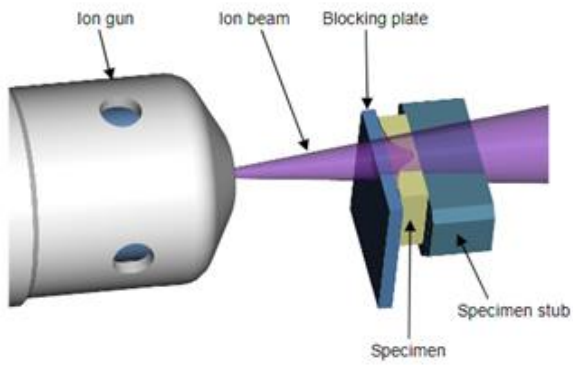

Figure 4. Cross-section milling setup [36]

3. Experimental Procedure

This section discusses the experimental setup, methodology and the procedures that were used to obtain the results.

3.1 Materials

Battery materials were obtained from two different commercial prismatic cells. These were NMC 622 and NMC 811 for the positive electrode and Graphite for the negative electrode. The cell also comprised of a polymer-based separator and Aluminum and Copper current collectors for the positive and negative electrodes, respectively.

3.2 Sample Preparation

The specimens were obtained from pristine and aged cells through Battery Teardowns, where the individual electrode materials were isolated in a Argon environment glovebox and specimen were cut with an office scissors from regions of interest as shown in Figure 5. Specimens were not rinsed, and no further treatment was carried out.

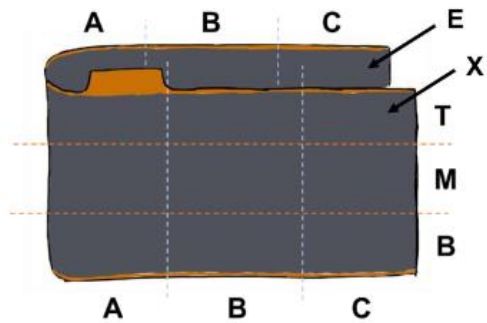

Figure 5. Labeling guide for specimens

The specimens for the method development were chosen from the first segment of the respective cells, where each segment is a length of 0.5 meters of electrode. The specimens chosen for location-based analysis was MA and TB according to the Figure 5. Whereas for studying Li Plating, samples were obtained from MA regions.

3.3 Broad Ion Beam Milling

Hitachi ArBlade 5000 was used to cross-section the samples. The parameters used for each material was optimized through method development. The method development was designed by varying the parameters of Acc. Voltage and Milling Time as shown in Table 2.

Table 2. Parameters for method development of BIB cross sectioning

Material	**Mill 1**		**Mill 2 (Cleaning/ Fine polishing)**	
	Acc. Voltage (kV)	Milling Time (hrs)	Acc. Voltage (kV)	Milling Time (hrs)
Positive Electrode	4.0	1.0		
	5.0	1.0		
	5.0	1.0	4.0	0.5
	5.0	1.5		
	5.0	2.0		
	6.0	0.5	4.0	0.5
	6.0	1.0		
	6.0	1.0	4.0	0.5
	6.0	2.0		
	7.0	1.0		
	7.0	2.0		

Graphite	6.0	0.5		
	6.0	0.5	4.0	0.5
	6.0	1.0		
	6.0	3.0		
	7.0	1.0		
	8.0	3.0		

The parameters developed from the method development were then used to analyze effects of aging. The aged electrode and Li plating samples were cross sectioned in an Argon environment. These samples were prepared in a glovebox and then transferred to the BIB in an airtight container, after cross-sectioning these were then transferred to the SEM using a custom-made airtight transfer chamber.

BIB was also used to produce slices of the same specimen for tortuosity measurements. Where the first slice was produced from the optimized parameters from the method development and the next two slices using 4kV with a milling time of 0.5hrs.

3.4 Scanning Electron Microscopy

Zeiss Sigma HD was used to image the cross-sectioned samples that were prepared from the BIB. The samples prepared in the airtight conditions used an airtight transfer chamber to transfer the specimen to the SEM. Whereas the non-airtight samples were mounted on regular stubs with carbon tape. Secondary Electron and Backscatter images were acquired with optimized working distance and accelerating voltages which were developed in conjunction with Image analysis and recommendation from the BIB manufacturer. The EDS maps were obtained at 15kV accelerating voltage.

3.5 Image Analysis

Raw Images obtained from the SEM are sources of large data that need to be quantitatively analyzed. These raw images were processed through ImageJ, in a stepwise manner as following and as summarized in Figure 6

1. The Raw images were either stitched or processed as it is, and were converted to 8-Bit format
2. The following were then thresholded based on the individual intensity level of the features of interest.
3. The image was then cleaned using despeckling and removing outliers the size of 1-2 pixels depending on the image
4. These were then segmented using the watershed feature to break up particles that appear large due to accumulation of smaller particles.

5. The parameters for the parameters for analysis were selected as follows, Area, Perimeter, Circularity and Equivalent diameter.

Figure 6. Image Analysis steps

The raw data obtained from the image analysis was then analyzed in MATLAB.

To summarize the Experimental procedure for studying the effects of ageing Figure 7 illustrates the stepwise procedure for obtaining the results. The sample is first cross sectioned using the BIB with the optimized parameters from the method development, and then analyzed in the SEM. Once the raw images are obtained from the SEM, these are analyzed in ImageJ. The raw data from the image analysis is then processed further and visualized in the data analysis step using MATLAB.

Figure 7. Experimental Procedure Summary

Tortuosity measurement required consecutive BIB-SEM use as summarized in Figure 8 Where each slice is made using the BIB and then imaged in the SEM, after total of three slices the raw images are stacked and analyzed in ImageJ and the Tortuosity is calculated using TauFactor applications.

Figure 8. Experimental Procedure for Tortuosity measurement

4. Results

The following section presents the results. It includes two sections, where the first section furnishes results of the method development for BIB, SEM and Image Analysis. The second section uses these results to analyze electrode morphology and effects of ageing.

4.1 Method Development

This section provides the results of the method development from the BIB, SEM, and Image Analysis. It provides optimized parameters that are recommended for cross-sectional analysis of electrode materials.

4.1.1 Broad Ion Beam Milling

The BIB is used to cross-section samples for observation in the SEM. The surface quality of the cross-section is dependent on the milling parameters of the BIB. These parameters are specific to the material and thickness of the specimen. Therefore, in order to prepare the samples for battery materials the parameters were optimized through both, input from the manufacturer of the BIB and also from carrying out deductive trials. The parameters that affect the quality of the mill are Acc. Voltage of the Ion beam and the milling Time. A combination of both these parameters were used as discussed in Table 2 , and then verified for surface quality. The results of the following parameters were then analyzed in the SEM as seen in Figure 9 . It is important to note that not all SEM images are captured with the same settings for the method development, since SEM parameters were concurrently being developed.

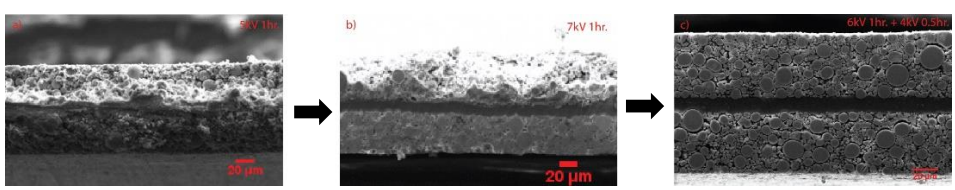

Figure 9. Positive electrode Cross-section produced with milling parameters a)5kV for 1 hr. b)7kV for 1 hr. c)6kV for 2 hr.

The SEM micrographs are evaluated qualitatively based on two criteria. Where the main criteria is the surface quality and the second is to minimize milling time. It is observed that increasing the milling time produces a deeper cut, this can be seen from the horizontal progression of the images . Whereas increasing the Acc. voltage increases the roughness of the cut, this is visible from the beam lines on the surface and increasing edge breakoff as observed with Figure 9 b). Therefore, to reduce the edge breakoff but also mill the surface a median value of 6kV was chosen. A second step of low voltage milling provides a high quality polished surface. It can be seen from the

Figure 9 c) that the milling lines have disappeared and therefore this method does indeed produce better surface finish.

Therefore, for the NMC811 positive electrode an accelerating voltage of 6kV was sufficient and a milling time of 0.5hrs was selected for reduced time, which is followed by low voltage (4kV) milling for 0.5hr. For the case of NMC622 positive electrode, it was observed that it was thicker than the NMC811 electrode and therefore increasing the milling time would be sufficient. Therefore, for NMC622 positive electrode an accelerating voltage of 6kV was sufficient and a milling time of 1hr was selected, followed by low voltage (4kV) milling for 0.5hr.

In the case of the Graphite Negative Electrode, it was challenging to obtain repeated results due to the interaction of graphite with the beam, which is primarily due to the flaky structure of graphite that produces an uneven surface. Multiple combinations of Acc. voltage and milling times were attempted.

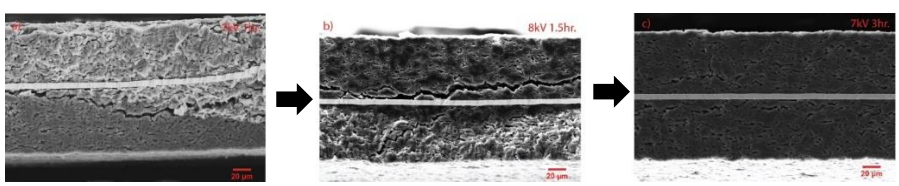

Figure 10. Negative electrode Cross-section produced with milling parameters a)7kV for 1 hr. b)8kV for 1.5hr. c)6kV for 3 hr.

It was observed from Figure 10. that increasing milling time produced a better surface finish. Although at higher voltage the mask was being consumed at a much faster rate and hence could not be reused after a single cross section. Therefore, an accelerating voltage of 6kV and a milling time of 3hrs was selected for an acceptable surface finish and least amount of damage to the mask.

The optimum parameters are summarized in the Table 3. Optimal parameters for Electrode materials for each material. These parameters are then used for analyzing the effects of aging on the battery materials.

Table 3. Optimal parameters for Electrode materials

Material	**Mill 1**	**Mill 2 (Fine polishing)**

	Acc. Voltage (kV)	Milling Time (hrs.)	Acc. Voltage (kV)	Milling Time (hrs.)
Positive Electrode (NMC622)	6.0	1.0	4.0	0.5
Positive Electrode (NMC811)	6.0	05	4.0	0.5
Negative Electrode	6.0	3.0		

4.1.2 Scanning Electron Microscopy

SEM Micrographs are crucial for accurate analysis of the microstructure. It is evident that two major factors play a role in the quality of the image, which is the accelerating voltage and the working distance. It was recommended from the manufacturer that low accelerating voltages and working distance (<2kV and <4mm) should be used for imaging battery materials. Although due to the limitations of the equipment, this was not the achievable. One of the contributing factors was the holder for the non-air tight specimens was prone to vibrations from the electron beam. It was also observed that reducing the Acc. Voltage reduces the visibility of the topological features, mainly the edges effect and the milling lines. Therefore with an accelerating voltage of 15kV and a working distance of <7 mm and was used for analysis. For the analysis of separator and Li plating, it was possible to achieve a low accelerating of 2kV and a working distance of <4mm as these samples were analyzed in the airtight holder.

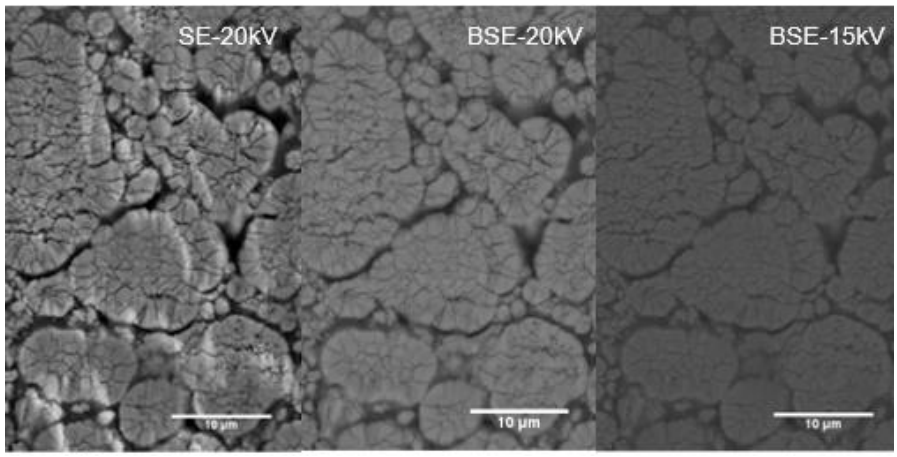

Figure 11. SEM Micrograph comparison between SE and BSE with Acc. voltage

SEM micrographs directly affect the outcome of the image analysis. Increased noise and milling lines reduces the ability to segment images and also reduces the accuracy of the shape factor and size calculations. It was observed from Figure 11 that imaging through BSE detector produced much smoother images although edge details were compromised, but this draw back did not affect the segmentation. Therefore BSE micrographs were adopted for image analysis.

4.1.3 Image Analysis solutions

Image analysis is used to measure the particle sizes and their shape factors. There were two solutions available, namely Zeiss ZenCore at Scania and ImageJ at Lund University. Both solutions provided segmentation and analysis although ZenCore was based on proprietary Machine Learning algorithm which required training with multiple images by marking areas of interest. ImageJ on the other hand provides built in tools for complex analysis which could be manually adjusted according to usage.

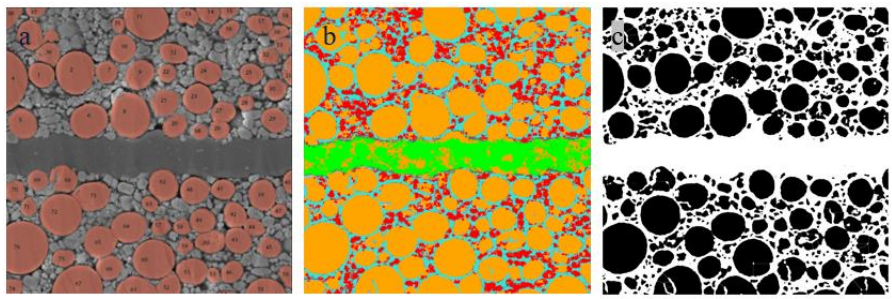

Figure 12. Comparison of results from a) Golden Sample b) ZenCore c) ImageJ

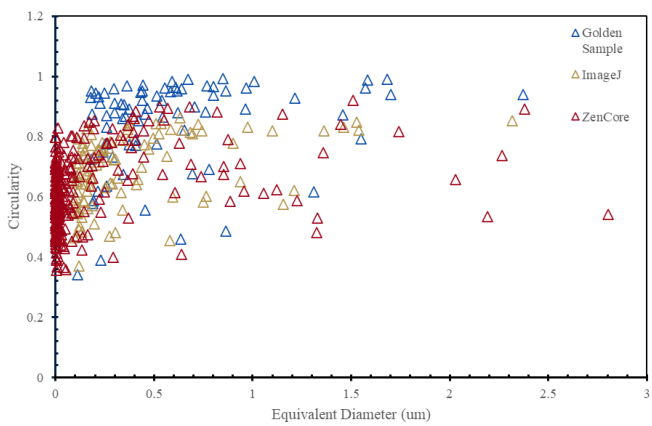

Figure 13. Plot of Circularity vs Equivalent diameter for comparison o ImageJ and ZenCore wth goldne sample

In order to compare the accuracy of these methods, a golden sample was designed by manually measuring the areas and perimeter of the large particles. The golden sample was then used to compare the analysis from ImageJ and ZenCore which is illustrated through Figure 12. It is evident through the comparison of circularity and equivalent diameter from Figure 13 that the segmentation in ImageJ is much better than ZenCore, as it struggles to separate particles., since there are considerable outliers of the equivalent diameter compared to the golden sample and ImageJ. ZenCore also has difficulty separating smaller particles and the current collector, it also struggles with measuring perimeter which directly affects the circularity . Therefore, overall due to better segmentation and accuracy, ImageJ has been used for image analysis.

4.1.4 Tortuosity Measurement

Tortuosity measurements required consecutive cross sectioned layers and simultaneous SEM imaging. The first layer was cross-sectioned using the parameters in Mill 1 as illustrated in Table 3. followed by SEM imaging of the cross-sectioned surface, and then further slices were obtained from the BIB using parameters from Mill 2 (fine polishing) and were consecutively micro graphed in the SEM. The distance between the layers is also measured using the SEM. These micrographs were then stacked in ImageJ to from a layered 3D image and the entire stack is then Thresholded and segmented. Lastly it is exported to the TauFactor Application for tortuosity measurement.

4.2 Electrode morphology and Effect of Aging

Electrode morphology differs depending on the recipe of manufacturing. As stated previously, there are two cells from different commercial manufacturers that will be observed, where one is NMC811 positive electrode with graphite as negative electrode and the second with NMC622 positive electrode with graphite negative electrode, this would mean different particle sizes, shapes, tortuosity and electrode dimensions. This difference is also expected to be observed with aging. The following section evaluates these changes.

4.2.1 NMC622 and NMC811 Pristine Electrodes

4.2.1.1 Positive Electrode

Dimensions

Electrode dimensions are expected to differ between two different electrode since they are manufactured by different companies, this is illustrated through SEM micrographs of cross sections from the BIB in Figure 14.

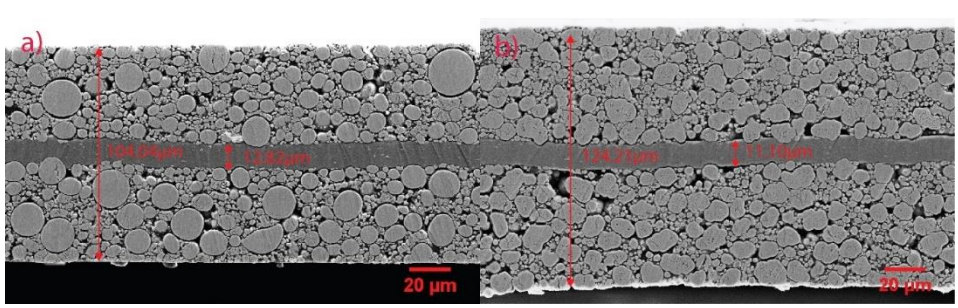

Figure 14. Micrographs of cross-sections of a) NMC811 b)NMC622

It is observed from Figure 14 that the NMC622 electrode is wider compared to the NMC811 electrode . This observation is verified from Image analysis in Table 4. , which confirms that the NMC622 Electrode is approximately 20% wider than the NMC811 Electrode.

Table 4. Electrode Dimensions for NMC811 and NMC622

	NMC811	**NMC622**
Electrode	104.04 ± 0.55	124.21 ± 0.92
Current Collector	12.82 ± 1.17	11.10 ± 0.90

Particle size and shape factors

The difference in particle size and shapes are expected as they are manufactured differently and have different recipes. The microscture of the electrodes are illustrated in Figure 15

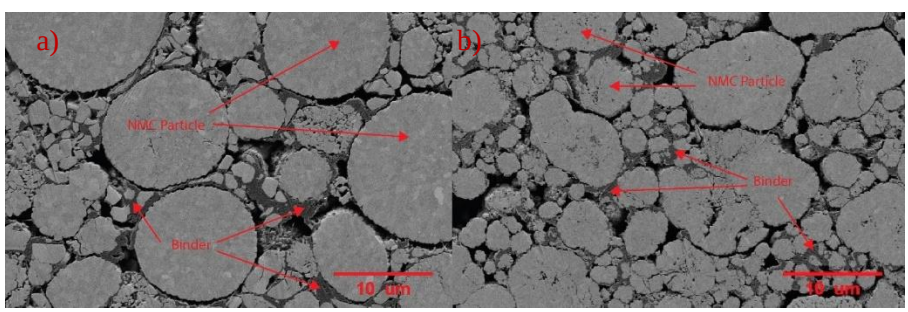

Figure 15. Particle micrograph of a) NMC811 b) NMC622

An observation can be made for the particle shapes and sizes, where NMC811 is composed of both large circular particles and smaller irregular particles which are held together with a binder. However in contrast, from the micrographs of NMC611, it is composed of relatively less circular large and slightly more circular small particles, although this is observation is from visual inspection of Figure 14. where the irregular particles are assumed to possess higher aspect ratios and lower circularity.

Image analysis of the micrographs provides evidence of a 'bi-modal' particle size in NMC622 whereas for NMC811 the particles are spread without much drastic variation across the range of the Equivalent diameter as observed from Figure 16. In the case of the particle shapes, image analysis contradicts the previous visual observation, since on average NMC622 particles are 6.25% more circular, this finding contradicts the previous observation. Upon analyzing the overall spread of the data, it is also seen from Fig a, that smaller sized particles, i.e., particles with lower equivalent diameters tend to be less

circular. In addition to this it is seen from Figure 17 a) b) that are more NMC811 outliers for circularity <0.4 which makes the overall statistics skewed. Therefore, it can be reasoned that NMC622 is composed of higher percentage of smaller circular particles which affects its overall higher circularity.

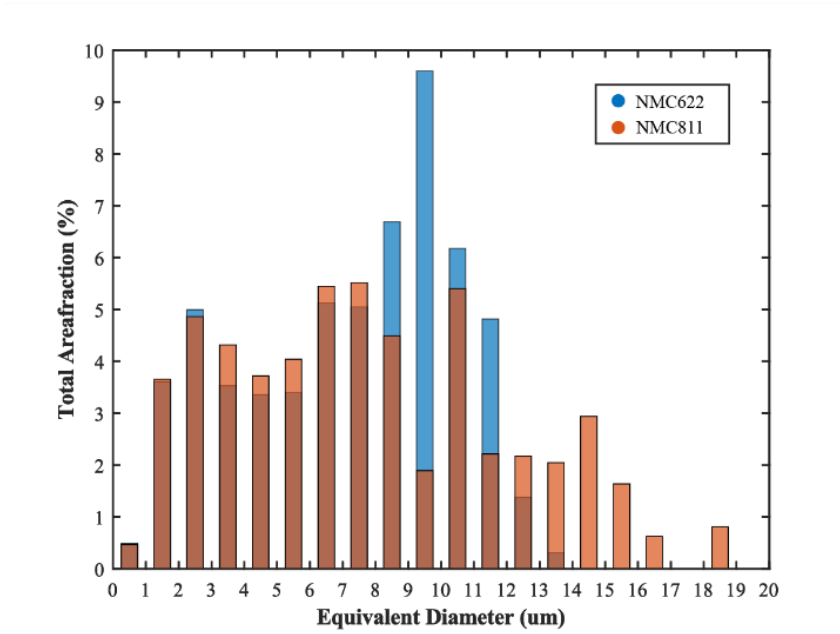

Figure 16. Distribution of equivalent diameter with the total fraction of area of the particles

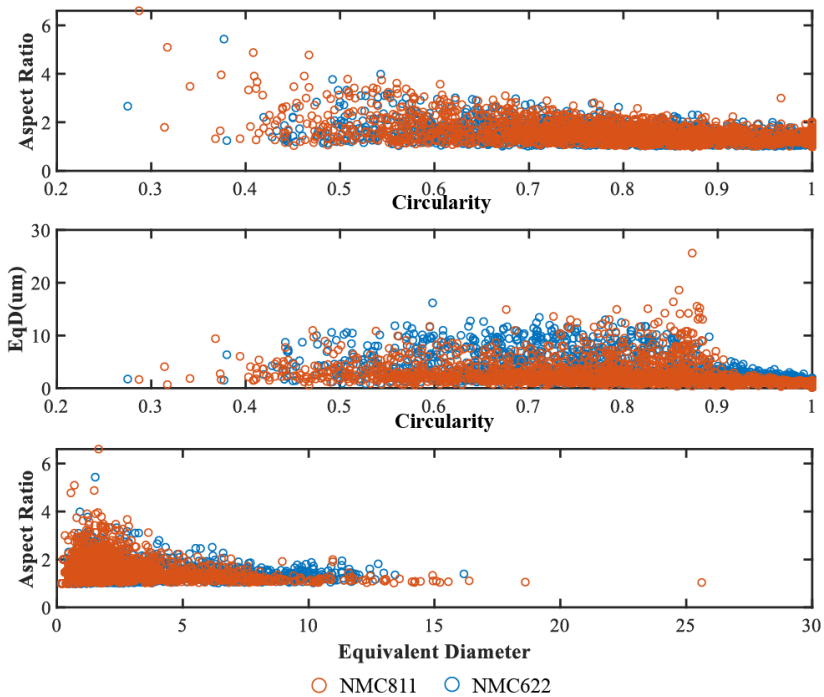

Figure 17. Plot of the a) Aspect ratio b) EqD against the diameter, and c) plot of aspect ratio against the equivalent diameter.

Tortuosity measurement

The NMC electrodes were then cross sectioned consecutively three times in order to obtain equidistant slices to reproduce the microstructure in 3D space. These slices are represented in Figure 18.

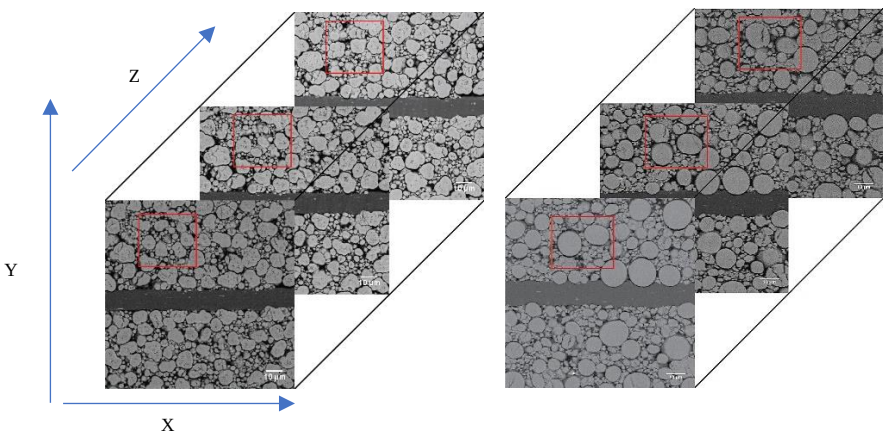

Figure 18. Cross section slices of NMC811 and NMC622 Electrode where the marked region denotes the area of analysis

The slices in Figure 18. were then stacked and measured for tortuosity which is represented in Table 5. It is observed that the overall tortuosity is higher in the case of the NMC622 for the X and Y directions

Table 5. Tortuosity Measurement for NMC811 and NMC622 Electrodes

	Tortuosity			**Porosity**
	X direction	Y direction	Z direction	
NMC811	2.55	2.26	3.38	32.8%
NMC622	3.41	2.87	2.51	36.3%

It is important to note that the thresholding of the image affects the porosity which consequently affects the tortuosity measurements. Therefore, there is a need to quantify this effect to accurately measure the values. The slices in Figure 18 have been thresholded between 90 and 150 units of intensity and then measured for tortuosity and porosity and results are published in Figure 19.

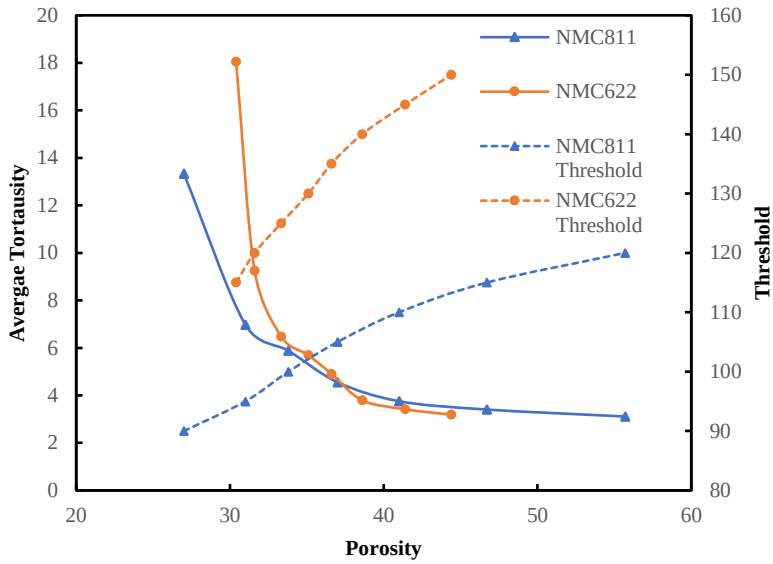

Figure 19. Tortuosity vs Porosity plot with Thresholding

It is evident from the Figure 19 that the relationship between Porosity and Tortuosity is an exponential function. This relationship helps to calculate Tortuosity when porosity is measured using other techniques or provided from the manufacturer.

4.2.1.2 Negative Electrode

Dimensions

Graphite flakes are used as the negative electrode for both the corresponding NMC622 and NMC811 samples. The micrographs of the cross-sections are displayed in Figure 20.

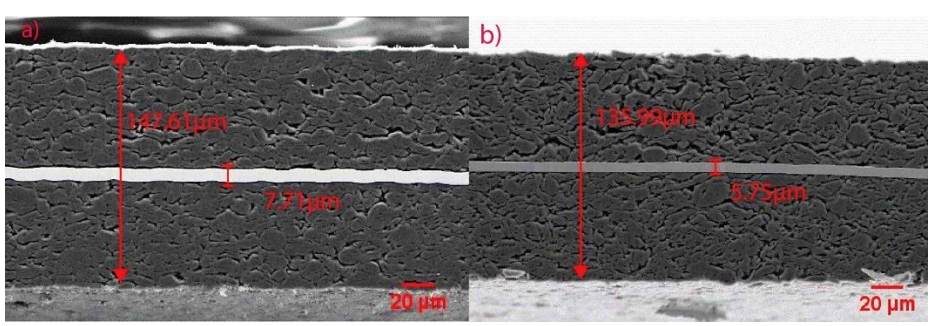

Figure 20. Microstructure of Graphite negative electrode corresponding to a) NMC811 b) NMC622

It is evident from Figure 20. that there is an increase in the thickness of the Negative electrode corresponding to NMC622. This is quantified in Table 6., where it is measured to have a 8.5% higher thickness.

Table 6. Graphite electrode dimensions

	Graphite (NMC811)	**Graphite (NMC622)**
Electrode	135.99 ± 1.68	147.6 ± 1.13
Current Collector	5.75 ± 0.23	7.71 ± 0.16

Particle size and shape factors

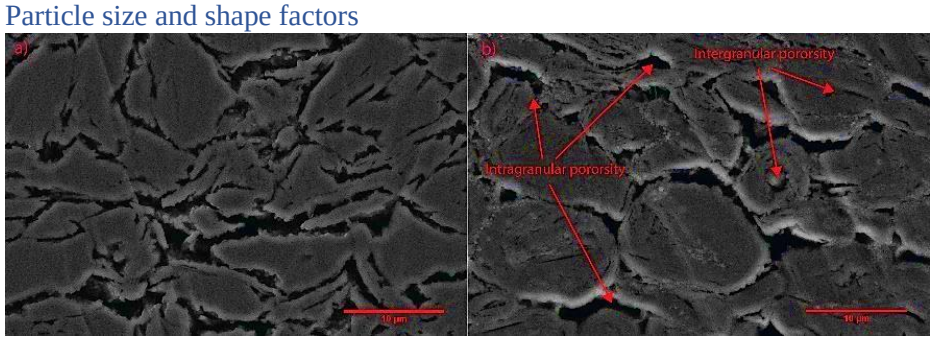

Figure 21. Particle shape comparison of graphite negative electrodes that correspond with a) NMC811 b)NMC622

It is seen from Figure 20, that the graphite flakes corresponding to the NMC622 wound up in a grain like feature. Whereas for graphite flakes corresponding to NMC811, it appears to be continuous shred of graphite with sharp edges. It is also visible that the graphite flakes (NMC622) have both an internal porosity within the grain and an external porosity between the grains. Overall only porosities are quantifiable and are represented in Table 7. Porosity is higher in the Graphite electrode corresponding the NMC622.

Table 7. Porosity Measurement

	Graphite (NMC811)	**Graphite (NMC622)**
Porosity (Area %)	10.36%	11.34%

4.2.2 Pristine vs Aged Electrodes

This section quantifies the effect of aging in electrodes. It is important to reiterate that only NMC622 Positive electrode and its corresponding Graphite electrode were aged and following are the results.

4.2.2.1 Positive Electrode

Dimensions

The positive electrode is expected to expand with aging. This is also followed by particle cracking as seen in Figure 22. The width of the electrodes are measured and quantified in Table 8. It is observed that there is that there is an increase in the thickness of the electrode by approximately 7.3% for TB and 11.8% for MA compared to pristine. This has been observed depending on location, and therefore two likely positions were chosen for the analysis as described previously. The micrographs for the cross-sections of location IMA and ITB are displayed in

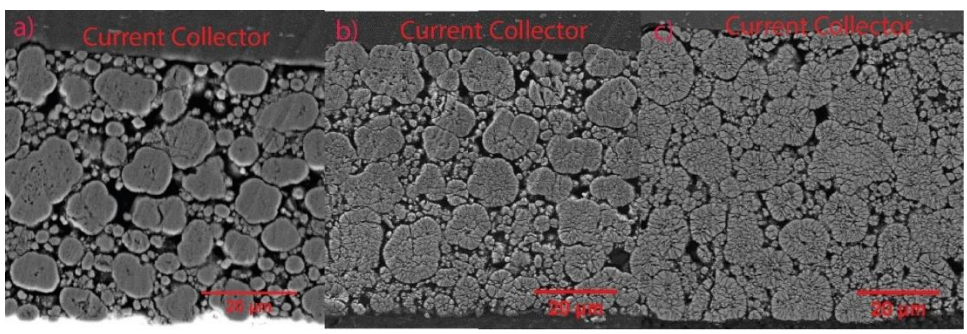

Figure 22. Electrode microstructure of NMC 622 a) Pristine b) Aged MA c)Aged TB

Table 8. NMC622 Pristine and Aged Dimensions

	NMC622 Pristine (µm)	**NMC622 Aged (ITB) (µm)**	**NMC622 Aged (IMA) (µm)**
Electrode	124.21 ± 0.92	133.21 ± 0.92	138.82 ± 1.57
Current Collector	11.10 ± 0.90	11.06 ± 0.89	11.10 ± 0.49

Particle size and shape factors

Particle cracking is a dominant effect seen from the micrographs in Figure 22. Particle cracking leads to a decrease in particle size and an increase in number of particles. The particle cracking is visible closer to the edges of the electrode for location TB. Although for MA it can be seen that the for entirety of the particles are cracked. This leads to an expected increase in the dimensions of the electrode. It is understood from Table 8. This is fits the trend in the observed increase of particle cracking with increase in electrode dimension.

Table 9. NMC622 Pristine and Aged Dimensions

	NMC622 Pristine (µm)	NMC622 Aged (ITB) (µm)	NMC622 Aged (IMA) (µm)
Electrode	124.21 ± 0.92	133.21 ± 0.92	138.82 ± 1.57
Current Collector	11.10 ± 0.90	11.06 ± 0.89	11.10 ± 0.49

Image analysis is used to quantify this observed increase in particle cracking. It is seen from Figure 25, 22 and 23 that with more particle cracking there is a considerable decrease in the Equivalent diameter and its spread with the increase in the number of particles. Some general deductions can be made from the Figure 25 that particle cracking leads to lower circularity, higher aspect ratios and lower equivalent diameter. There is a 9.6 % decrease in circularity, 13.6% increase in aspect ratio and 89.3 % decrease in equivalent diameter for IMA whereas for ITB there is 11.0 % decrease in circularity, 10.1% increase in aspect ratio and 84.1 % decrease in equivalent diameter.

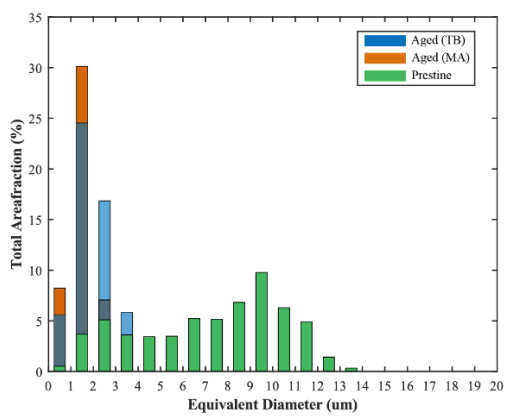

Figure 23. Particle size distribution with area fraction for aged (MA and TB) and pristine electrodes

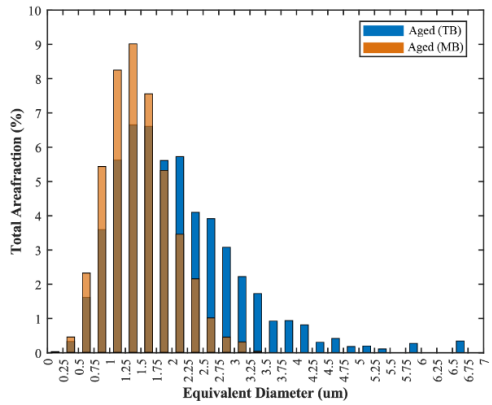

Figure 24.Particle size distribution with area fraction for MA and TB regions

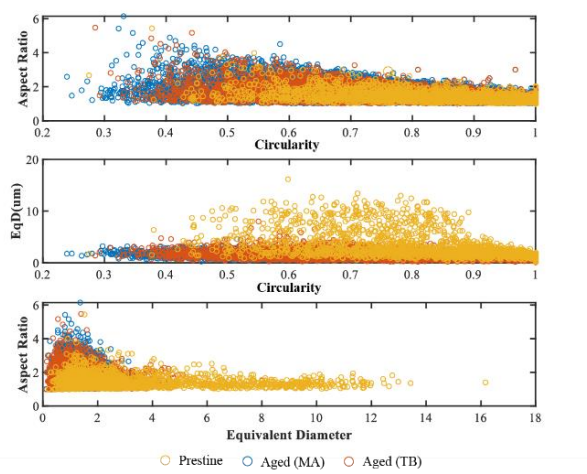

Figure 25. Particle Shape Analysis for aged and pristine electrodes

It is interesting to note that the observation of larger particle cracking closer to the edges of the electrode for location ITB, coincides with the wider spread of the data in Figure 24 compared to IMA. Therefore, there is an need to evaluate this trend along the thickness of the electrode. In order to do so, both IMA and ITB have been divided into six regions as illustrated in Figure 26

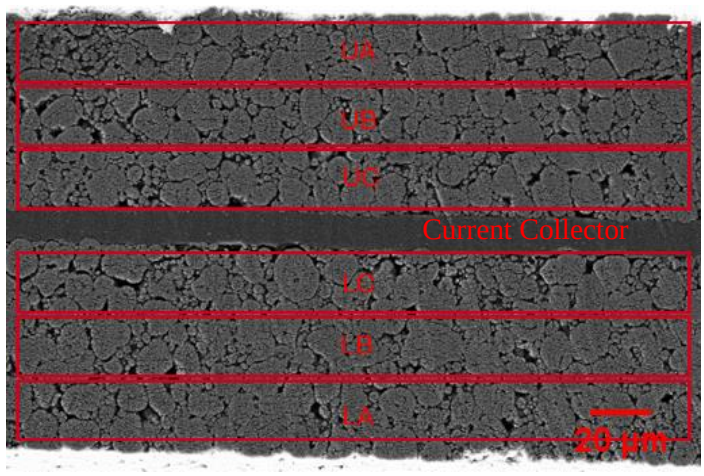

Figure 26. Distribution of Areas for analyzing location based particle cracking

It is expected to observe higher equivalent diameter for the UC and LC regions of ITB whereas for IMA, all the regions are expected to have similar equivalent diameter. The image analysis result in Figure 15, plots the trend of the equivalent diameter with the proximity to the current collector. It proves that equivalent diameter is highest near the current collector at UC and LC for both IMA and ITB. Contrary to the visual observation for IMA, there is a trend of decrease in the particle size with location away from the current collector and closer to the edge/separator. Hence it can be concluded that there is differential cracking of particles depending on location, where the particle closes to the current collectors experience less cracking than on the edges.

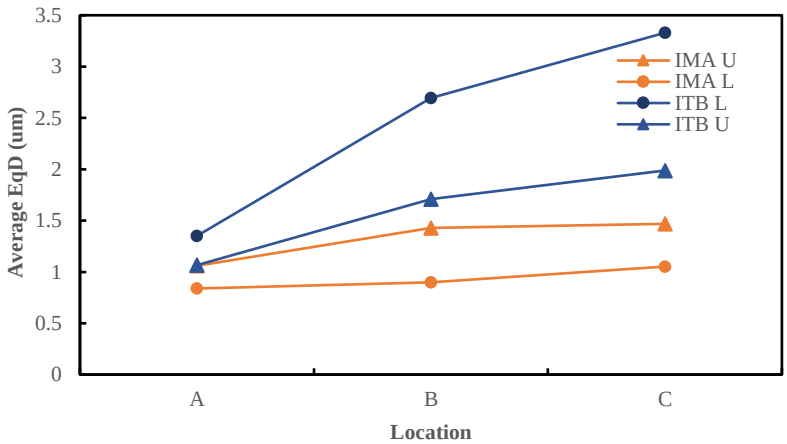

Figure 27. Equivalent diameter based on Location of Aged NMC622

Tortuosity measurement

The aged electrodes were cross sectioned consecutively three times in order to obtain equidistant slices to reproduce the microstructure in 3D space. These images were then stacked and segmented and then measured for tortuosity. The overall tortuosity has decreased with aging as seen from Table 10, this is due to the particle cracking and therefore increased porosity which enable shorter travel paths.

Table 10. tortuosity measurement of aged and pristine NMC622 electrodes

	X direction	**Y direction**	**Z direction**
NMC622 (Aged)	2.39	1.83	2.10
NMC622 (Pristine)	3.41	2.87	2.51

4.2.2.2 Negative Electrode

Dimensions

Effect of ageing is expected to show on the electrode morphology, this is visible from the micrographs in Figure 28. It is observed that with ageing there are not only cracks in the graphite electrode but also delamination from the current collector.

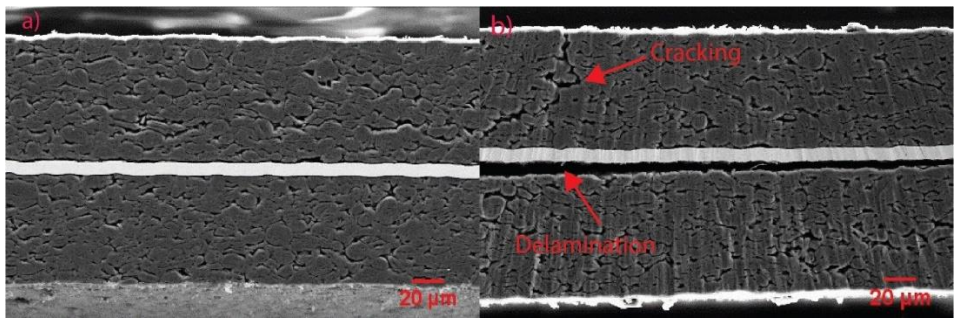

Figure 28. Microstructure of Graphite Negative electrode corresponding to NMC622 a)Pristine b)Aged

The aged electrode has increased in thickness by 2.83% while the porosity has been reduced by 9% . Although unlike the positive electrode, an inverse relation between the thickness and porosity would mean that there are other phenomenon causing this effect.

Table 11. Negative Electrode Dimensions and Porosity

	Graphite Pristine	**Graphite Aged**
Electrode	147.6 ± 1.13	151.78 ± 1.63
Current Collector	7.71 ± 0.16	7.45 ± 0.34
Porosity (Area %)	11.34%	10.31%

Li plating

Aging of electrodes leads to the formation of Li plating on negative electrode. This effect is studied by analyzing the cross-ssections of the graphite electrode with the separator attached from the regions of Li plating as shown in Figure 29

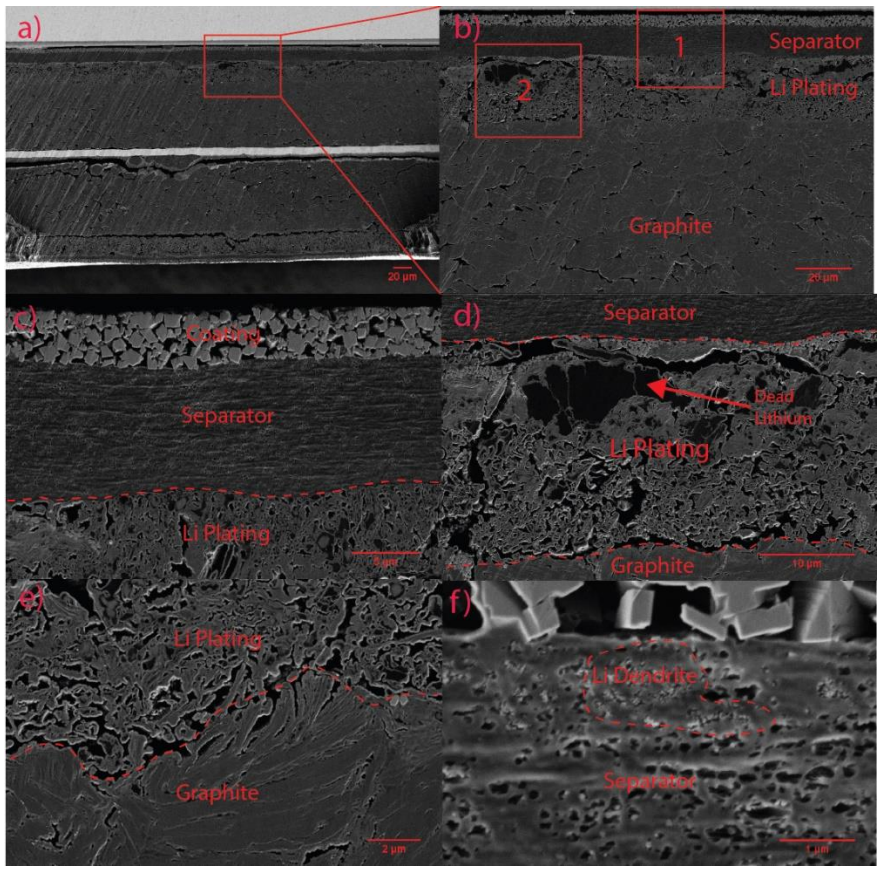

Figure 29. Micrographs of Li Plating region a)Electrode over view b)Area of Interest c)Separator (1) d)Li plating Region (2) e) Li plating boundary f) Li dendrite in separator

The specimen in Figure 29. is a collective cross section of the separator and the negative electrode. This is composed of two layers of coatings as seen in Figure 29 c) where the separator shares its edges with and Aluminum oxide coating of thickness 3.8µm on the top and a thinner layer of smaller particle size Al_2O_3 coating (inner) against the graphite electrode. These coatings are present to prevent the Li dendrites to penetrate the separator and reach the other side to cause short circuits. The separator is a porous polymer of thickness 10.6µm. It can also be observed from closer inspection in Figure 29 f), that the separator contains insertions which are visible through the pores. These are assumed to be Li dendritic growth through the separator although it could not be verified. The EDS map in Figure 30 is used to confirm the presence of Li plating, although it cannot detect Li, it is seen that the region is devoid any other active material composition. It is also composed of phosphorus and fluorine, which are elements that compose the

electrolyte. The formation of Li plating consumes the electrolyte and hence there is abundant trace of these elements in the region. Therefore, it is assumed to be Li plating based on location and EDS spectra.

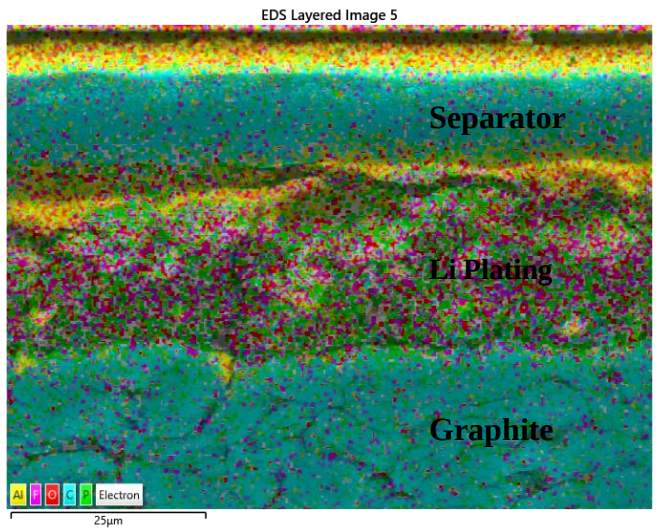

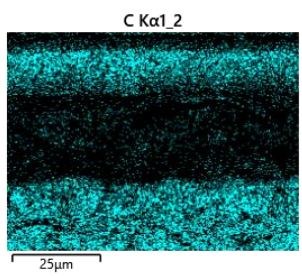

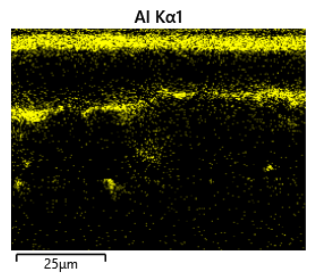

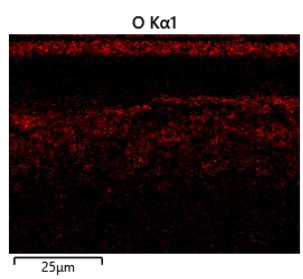

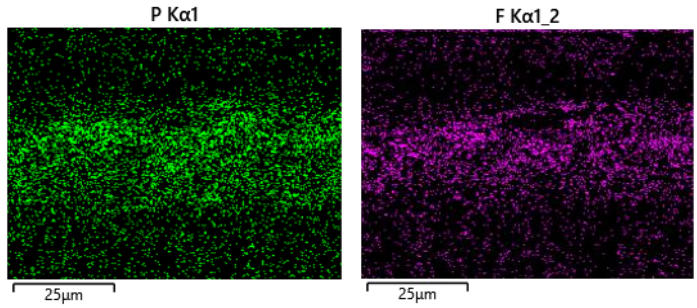

Figure 30. EDS Map of Aged Graphite Negative Electrode

The Li plating has a thickness of 22.34µm, which originates from the graphite as seen in Figure 29 c) d). and makes contact with the separator and the inner coating. Although for this sample the inner coating seems to have been fragmented and is embedded inside the Li plating region. The lithium plating region is composed of filiform dendritic growth from the graphite which also includes larger uniform regions in the core as seen from Figure 29 d). These regions are assumed be dead Lithium masses that are a by-product of the aging mechanism.

5. Discussion

5.1 NMC 622 vs 811 electrodes

The two electrodes were sourced from cells that were produced by different manufacturers and were made with different recipes. Nevertheless, evaluating these electrodes provides insight into the cell design and delivers input for further numerical modelling. The NMC622 electrode are thicker and more porous, the positive and negative electrodes are 20% and 8.5% wider on average respectively. A thicker electrode would imply a higher energy density and lower power density, although various other factors such as porosities, content of inactive material and chemical composition also affects the electrochemical performance [37]. Evidently from the results there is a decrease in the content of inactive material like the current collector which is reduced in size by approximately 13.4%, the same could not be assumed of the binder material as it was difficult to evaluate. Both electrodes also differ based on the particle size and shape factors. NMC622 as a bimodal distribution with a higher average equivalent diameter to that of NM811, although to make better statistical evaluation, the NMC622 particles possess lower 99^{th} and 50^{th} percentile equivalent diameter although lower 50^{th} and 5^{th} percentile circularity. These translate to larger particles being more circular for both the electrode and the smaller particles being more irregular

in NMC822 compared to NMC622. The NMC622 particles are also packed more efficiently with larger area fraction, denoting higher fraction of active material.

The porosity of the NMC622 electrode is higher for both the positive and its corresponding negative electrode. Although it is important to note that there are limitations in measuring porosity through image analysis, particularly for the negative electrode as it requires higher resolution imaging. Increasing cathode porosity would mean lower energy density and rate capability, although an optimal range of porosity and corresponding thickness would provide the highest energy density [38]. The porosity and tortuosity are related through the Bruggeman relationship. A higher porosity would mean a lower tortuosity and vice versa, since increasing porosity creates expanding spaces that provide the ability for the particle to travel shorter paths. Therefore, using this relationship, knowledge of one porosity can help determine tortuosity. Porosity can be calculated through methods such as pycnometer or BET etc., nevertheless the porosity value for NMC622 is reported to be 38%, which was provided by the Battery Cell Development Team (UBCM) at Scania. Therefore, from this input it can be claimed that the Tortuosity factor for Pristine NMC622 is 3.88, which is higher than NMC811 which possess a tortuosity of 4.35 at the same porosity level.

5.2 Pristine vs Aged Electrode

The pristine and aged electrodes from the NM611 based cell were analyzed, and both positive and negative electrodes experienced an increase in cell dimensions between 7.3% to 11.8% for the cathode and 10.3% increase for the anode with aging. This effect is expected since repeated cyclic insertion and extraction of Li ions causes volume change, this then leads to further mechanical failure in both the electrodes such as diffusion induced stress, crystal distortion in NMC, crack growth and nucleation [11]. Particle cracking has been the most noticeable effect of ageing, this has been the predominant observation in the positive electrode from the SEM micrographs. At the individual particle level, Aged NMC particles display cracks that originate from the center and propagate towards the sides. These cracks are expected to be a result of the phase conversion that causes fracturing. This can lead to poor electrical conductivity due to loss of contact and acceleration of side reactions due to new sites and surfaces that are generated [39].

A trend in the particle cracking based on location has also been observed at the electrode level. Particles closer to the edge of the electrode tend to be more cracked than the ones closer to the current collector. This is explained by the porous electrode theory where the surface potential is highest closer

to the electrode edge or separator, this region also has higher electron transfer density and well as Li flux [40]. The particles closer to the separator have been reported to experience higher SoC compared to the current collector, this region is also highly lithiated closer to the separator and hence is expected to experience severe phase transition which causes higher levels of particle cracking [41]. The same effect is seen with different regions, cross-sections of electrode closer to the tab tend to be more cracked than regions further from it, the same reasoning of difference in current densities would be the cause of this effect. Particle cracking causes an expected increase in porosity and a reduction in tortuosity for the positive electrode. Whereas for the negative electrode there is an observed reduction in porosity. This reduction could be explained by the growth of a surface film , which is contributed by formation of SEI and Li plating [42].

Li plating is observed on the negative electrode that is cross sectioned with the separator. It is evident that the observed filiform like structured layer of thickness of 22.34um is indeed Li plating due it location between the edge of the graphite negative electrode and the separator. The EDS map also proves major elements present in the region are by-products of the electrolyte that was consumed. Li plating accelerate the further growth of SEI layer and forms dead lithium regions which are assumed to be visible in the micrographs but are could not be proven [43]. Lithium insertions have also been found in the porous separator where it has penetrated the separator and are visible through the pores. These dendrites can be concerning as it can perforate the separator and reach the other side causing short circuits, although an Al_2O_3 coating of 3.8um is present to prevent this from occurring.

6. Conclusion

The aim of the thesis was to develop the methodology for BIB-SEM and image analysis characterization. The parameters for the BIB were developed for battery electrodes including separator and negative electrode sandwich. The image analysis and tortuosity measurement tools were also setup and standardized. These parameters were then used to analyze electrodes from different manufacturers and also quantify the effect of ageing. It was noted that NMC622 positive and negative electrode possessed lower tortuosity and higher porosity, thickness and over all higher equivalent diameter, circularity and aspect ratio compared to NMC811. In the case of the ageing the electrode displayed delamination, volume expansion, particle cracking and Li plating. The particle cracking exacerbated towards the edge or the separator side of the electrode and gradually reduced towards current collector. Li plating was also visualized, its filiform like morphology and the location were key in its

identification, which was also supported by the presence of electrolyte constituent in the layer. Regions of dead lithium in the Li plating region and Li dendrite were also spotted in the separator.

7. Future Work

The following areas can be further investigated

1. Measurement of Negative Electrode Tortuosity by building on the current techniques through creating multiple slices and high resolution imaging.
2. Shape factors to evaluate Negative electrode, where one suggestion could be to look into fractal dimension or other factors can be developed
3. Location based analysis of Li plating in different regions, as this was observed from the teardown that Li plating was profound near the edges
4. Correlate image analysis results with electrochemical measurements to verify observations and visualize mechanisms

References

[1] "Scania's electrification roadmap." [Online]. Available: https://www.scania.com/group/en/home/newsroom/news/2021/Scanias-electrification-roadmap.html. [Accessed: 27-May-2022].

[2] K. Liu *et al.*, "Electrochemical modeling and parameterization towards control-oriented management of lithium-ion batteries," *Control Eng. Pract.*, vol. 124, p. 105176, Jul. 2022, doi: 10.1016/J.CONENGPRAC.2022.105176.

[3] P. Roy and S. K. Srivastava, "Nanostructured anode materials for lithium ion batteries," *J. Mater. Chem. A*, vol. 3, no. 6, pp. 2454–2484, Jan. 2015, doi: 10.1039/C4TA04980B.

[4] M. K. Tran, A. Dacosta, A. Mevawalla, S. Panchal, and M. Fowler, "Comparative Study of Equivalent Circuit Models Performance in Four Common Lithium-Ion Batteries: LFP, NMC, LMO, NCA," *Batter. 2021, Vol. 7, Page 51*, vol. 7, no. 3, p. 51, Jul. 2021, doi: 10.3390/BATTERIES7030051.

[5] A. K. Stephan, “A Pathway to Understand NMC Cathodes,” *Joule*, vol. 4, no. 8, pp. 1632–1633, Aug. 2020, doi: 10.1016/J.JOULE.2020.08.004.

[6] H. Zhang, Y. Yang, D. Ren, L. Wang, and X. He, “Graphite as anode materials: Fundamental mechanism, recent progress and advances,” *Energy Storage Mater.*, vol. 36, pp. 147–170, Apr. 2021, doi: 10.1016/J.ENSM.2020.12.027.

[7] J. Asenbauer, T. Eisenmann, M. Kuenzel, A. Kazzazi, Z. Chen, and D. Bresser, “The success story of graphite as a lithium-ion anode material – fundamentals, remaining challenges, and recent developments including silicon (oxide) composites,” *Sustain. Energy Fuels*, vol. 4, no. 11, pp. 5387–5416, Oct. 2020, doi: 10.1039/D0SE00175A.

[8] A. Li *et al.*, “A Review on Lithium-Ion Battery Separators towards Enhanced Safety Performances and Modelling Approaches,” *Mol. 2021, Vol. 26, Page 478*, vol. 26, no. 2, p. 478, Jan. 2021, doi: 10.3390/MOLECULES26020478.

[9] C. R. Birkl, M. R. Roberts, E. McTurk, P. G. Bruce, and D. A. Howey, “Degradation diagnostics for lithium ion cells,” *J. Power Sources*, vol. 341, pp. 373–386, Feb. 2017, doi: 10.1016/J.JPOWSOUR.2016.12.011.

[10] K. C. Kam and M. M. Doef, “Electrode Materials for Lithium Ion Batteries | Energy Technology Area,” *Mater. Matters*, vol. 2, no. 4, 2012.

[11] C. Lin, A. Tang, H. Mu, W. Wang, and C. Wang, “Aging Mechanisms of Electrode Materials in Lithium-Ion Batteries for Electric Vehicles,” 2015, doi: 10.1155/2015/104673.

[12] S. E. J. O’Kane *et al.*, “Lithium-ion battery degradation: how to model it,” *Phys. Chem. Chem. Phys.*, vol. 24, no. 13, pp. 7909–7922, Mar. 2022, doi: 10.1039/D2CP00417H.

[13] D. P. Abraham, R. D. Twesten, M. Balasubramanian, I. Petrov, J. McBreen, and K. Amine, “Surface changes on LiNi0.8Co0.2O2 particles during testing of high-power lithium-ion cells,” *Electrochem. commun.*, vol. 4, no. 8, pp. 620–625, Aug. 2002, doi: 10.1016/S1388-2481(02)00388-0.

[14] S. Venkatraman, Y. Shin, and A. Manthiram, “Phase relationships and structural and chemical stabilities of charged Li1-xCoO2-δ and Li1-xNi0.85Co0.15O2-δ,” *Electrochem. Solid-State Lett.*, vol. 6, no. 1, p. A9, Jan. 2003, doi: 10.1149/1.1525430/XML.

[15] R. Jung *et al.*, “Nickel, Manganese, and Cobalt Dissolution from Ni-Rich NMC and Their Effects on NMC622-Graphite Cells,” *J. Electrochem. Soc.*, vol. 166, no. 2, pp. A378–A389, Feb. 2019, doi: 10.1149/2.1151902JES/XML.

[16] V. Agubra and J. Fergus, “Lithium Ion Battery Anode Aging Mechanisms,” *Materials (Basel).*, vol. 6, no. 4, p. 1310, 2013, doi: 10.3390/MA6041310.

[17] D. E. Brown, E. J. McShane, Z. M. Konz, K. B. Knudsen, and B. D. McCloskey, “Detecting onset of lithium plating during fast charging of Li-ion batteries using operando electrochemical impedance spectroscopy,” *Cell Reports Phys. Sci.*, vol. 2, no. 10, p. 100589, Oct. 2021, doi: 10.1016/J.XCRP.2021.100589.

[18] D. Linden and T. B. Reddy, *Handbook of batteries*, vol. 33, no. 04. 1995.

[19] H. Berg, *The electrochemical cell*. 2015.

[20] G. Liu, D. Wang, J. Zhang, A. Kim, and W. Lu, “Preventing Dendrite Growth by a Soft Piezoelectric Material,” *ACS Mater. Lett.*, vol. 1, no. 5, pp. 498–505, Nov. 2019, doi: 10.1021/ACSMATERIALSLETT.9B00289/SUPPL_FILE/TZ9B00289_SI_004.MP4.

[21] J. Steiger, D. Kramer, and R. Mönig, “Microscopic observations of the formation, growth and shrinkage of lithium moss during electrodeposition and dissolution,” *Electrochim. Acta*, vol. 136, pp. 529–536, Aug. 2014, doi: 10.1016/J.ELECTACTA.2014.05.120.

[22] C. T. Love, O. A. Baturina, and K. E. Swider-Lyons, “Observation of lithium dendrites at ambient temperature and below,” *ECS Electrochem. Lett.*, vol. 4, no. 2, pp. A24–A27, Jan. 2014, doi: 10.1149/2.0041502EEL/XML.

[23] C. Busà, M. Belekoukia, and M. J. Loveridge, “The effects of ambient storage conditions on the structural and electrochemical properties of NMC-811 cathodes for Li-ion batteries,” *Electrochim. Acta*, vol. 366, p. 137358, Jan. 2021, doi: 10.1016/J.ELECTACTA.2020.137358.

[24] T. Rauhala, K. Jalkanen, T. Romann, E. Lust, N. Omar, and T. Kallio, “Low-temperature aging mechanisms of commercial graphite/LiFePO4 cells cycled with a simulated electric vehicle load profile—A post-mortem study,” *J. Energy Storage*, vol. 20, pp. 344–356, Dec. 2018, doi: 10.1016/J.EST.2018.10.007.

[25] C. Uhlmann, J. Illig, M. Ender, R. Schuster, and E. Ivers-Tiffée, “In

situ detection of lithium metal plating on graphite in experimental cells," *J. Power Sources*, vol. 279, pp. 428–438, Apr. 2015, doi: 10.1016/J.JPOWSOUR.2015.01.046.

[26] Y. Yuan, K. Amine, J. Lu, and R. Shahbazian-Yassar, "Understanding materials challenges for rechargeable ion batteries with in situ transmission electron microscopy," *Nat. Commun. 2017 81*, vol. 8, no. 1, pp. 1–14, Aug. 2017, doi: 10.1038/ncomms15806.

[27] Z. Zeng, W. I. Liang, H. G. Liao, H. L. Xin, Y. H. Chu, and H. Zheng, "Visualization of electrode-electrolyte interfaces in LiPF 6/EC/DEC electrolyte for lithium ion batteries via in situ TEM," *Nano Lett.*, vol. 14, no. 4, pp. 1745–1750, Apr. 2014, doi: 10.1021/NL403922U/SUPPL_FILE/NL403922U_SI_003.AVI.

[28] H. Ge *et al.*, "Investigating Lithium Plating in Lithium-Ion Batteries at Low Temperatures Using Electrochemical Model with NMR Assisted Parameterization," *J. Electrochem. Soc.*, vol. 164, no. 6, pp. A1050–A1060, Mar. 2017, doi: 10.1149/2.0461706JES/XML.

[29] J. Arai and R. Nakahigashi, " Study of Li Metal Deposition in Lithium Ion Battery during Low-Temperature Cycle Using In Situ Solid-State 7 Li Nuclear Magnetic Resonance ," *J. Electrochem. Soc.*, vol. 164, no. 13, pp. A3403–A3409, Nov. 2017, doi: 10.1149/2.1921713JES/XML.

[30] F. Lin *et al.*, "Synchrotron X-ray Analytical Techniques for Studying Materials Electrochemistry in Rechargeable Batteries," doi: 10.1021/acs.chemrev.7b00007.

[31] M. Lang *et al.*, "Post mortem analysis of fatigue mechanisms in LiNi0.8Co0.15Al0.05O2 – LiNi0.5Co0.2Mn0.3O2 – LiMn2O4/graphite lithium ion batteries," *J. Power Sources*, vol. 326, pp. 397–409, Sep. 2016, doi: 10.1016/J.JPOWSOUR.2016.07.010.

[32] M. Ebner, D. W. Chung, R. E. García, and V. Wood, "Tortuosity Anisotropy in Lithium-Ion Battery Electrodes," *Adv. Energy Mater.*, vol. 4, no. 5, p. 1301278, Apr. 2014, doi: 10.1002/AENM.201301278.

[33] B. Tjaden, D. J. L. Brett, and P. R. Shearing, "Tortuosity in electrochemical devices: a review of calculation approaches," *https://doi.org/10.1080/09506608.2016.1249995*, vol. 63, no. 2, pp. 47–67, Feb. 2016, doi: 10.1080/09506608.2016.1249995.

[34] S. J. Cooper, A. Bertei, P. R. Shearing, J. A. Kilner, and N. P. Brandon, "TauFactor: An open-source application for calculating tortuosity factors from tomographic data," *SoftwareX*, vol. 5, pp.

203–210, Jan. 2016, doi: 10.1016/J.SOFTX.2016.09.002.

[35] R. Jiang, M. Li, Y. Yao, J. Guan, and H. Lu, “Application of BIB polishing technology in cross-section preparation of porous, layered and powder materials: A review,” doi: 10.1007/s11706-019-0457-0.

[36] “Hitachi Ion Milling System,” *Hitachi High Technologies Corporation* , 2013. [Online]. Available: https://www.hitachi-hightech.com/file/us/pdf/library/application/Hitachi_IM4000_Ion_Milling_E-Brochure_HTD-E197R.pdf. [Accessed: 27-May-2022].

[37] H. Zheng, J. Li, X. Song, G. Liu, and V. S. Battaglia, “A comprehensive understanding of electrode thickness effects on the electrochemical performances of Li-ion battery cathodes,” *Electrochim. Acta*, vol. 71, pp. 258–265, Jun. 2012, doi: 10.1016/J.ELECTACTA.2012.03.161.

[38] C. Heubner *et al.*, “Understanding thickness and porosity effects on the electrochemical performance of LiNi0.6Co0.2Mn0.2O2-based cathodes for high energy Li-ion batteries,” *J. Power Sources*, vol. 419, pp. 119–126, Apr. 2019, doi: 10.1016/J.JPOWSOUR.2019.02.060.

[39] P. Yan, J. Zheng, M. Gu, J. Xiao, J.-G. Zhang, and C.-M. Wang, “Intragranular cracking as a critical barrier for high-voltage usage of layer-structured cathode for lithium-ion batteries,” *Nat. Commun.*, 2017, doi: 10.1038/ncomms14101.

[40] A. M. Boyce *et al.*, “Cracking predictions of lithium-ion battery electrodes by X-ray computed tomography and modelling.”

[41] Y. Yang *et al.*, “Quantification of Heterogeneous Degradation in Li-Ion Batteries,” 2019, doi: 10.1002/aenm.201900674.

[42] X. G. Yang, Y. Leng, G. Zhang, S. Ge, and C. Y. Wang, “Modeling of lithium plating induced aging of lithium-ion batteries: Transition from linear to nonlinear aging,” *J. Power Sources*, vol. 360, pp. 28–40, Aug. 2017, doi: 10.1016/J.JPOWSOUR.2017.05.110.

[43] J. S. Edge *et al.*, “Lithium ion battery degradation: what you need to know,” *Phys. Chem. Chem. Phys.*, vol. 23, no. 14, pp. 8200–8221, Apr. 2021, doi: 10.1039/D1CP00359C.